Chem

CellPress

Article

The tension-activated carbon–carbon bond

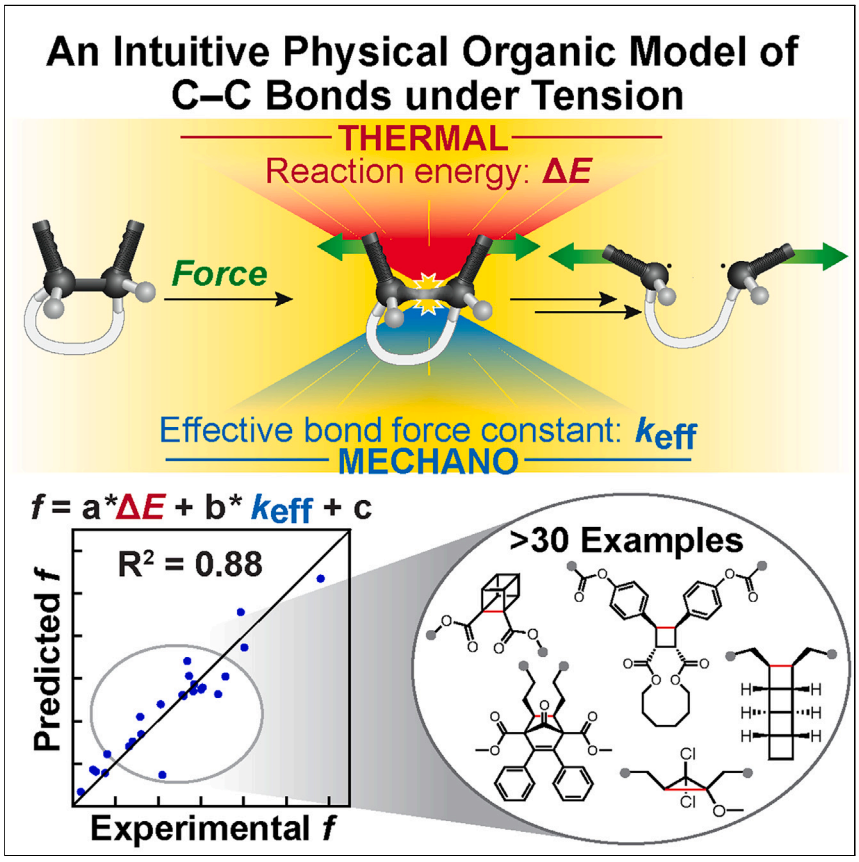

An intuitive physical organic model was developed to understand and predict the reactivity of C–C bonds under tension by leveraging two key molecular features: the effective force constant of the scissile bond (k_{eff}) and the force-free reaction energy (ΔE). Lower ΔE values suggest more favorable thermal reactivity, whereas lower k_{eff} values indicate improved mechanochemical coupling. A multivariate linear model was also established to predict the transition force (f^*) of more than 30 C–C bonds in various mechanophores.

Yunyan Sun, Ilia Kevlishvili, Tatiana B. Kouznetsova, Zach P. Burke, Stephen L. Craig, Heather J. Kulik, Jeffrey S. Moore

stephen.craig@duke.edu (S.L.C.)
hjkulik@mit.edu (H.J.K.)
jsmoore@illinois.edu (J.S.M.)

Highlights

Two key molecular features k_{eff} and ΔE inspired from the Morse potential

Structure-reactivity relationships of four norborn-2-en-7-one (NEO) mechanophores

Connecting k_{eff} and ΔE with state-of-the-art simulations

A multivariate linear model to generally predict f^* of C–C bonds

Sun et al., Chem *10*, 1–12
October 10, 2024 © 2024 Elsevier Inc. All rights are reserved, including those for text and data mining, AI training, and similar technologies.
https://doi.org/10.1016/j.chempr.2024.05.012

Please cite this article in press as: Sun et al., The tension-activated carbon–carbon bond, Chem (2024), https://doi.org/10.1016/j.chempr.2024.05.012

Chem

CellPress

Article

The tension-activated carbon–carbon bond

Yunyan Sun,[1,2,6] Ilia Kevlishvili,[3,6] Tatiana B. Kouznetsova,[4] Zach P. Burke,[1] Stephen L. Craig,[4,*] Heather J. Kulik,[3,5,*] and Jeffrey S. Moore[1,2,7,*]

SUMMARY

Mechanical force drives distinct chemical reactions; yet, its vectoral nature results in complicated coupling with reaction trajectories. Here, we utilize a physical organic model inspired by the classical Morse potential and its differential forms to identify effective force constant (k_{eff}) and reaction energy (ΔE) as key molecular features that govern mechanochemical kinetics. Through a comprehensive experimental and computational investigation with four norborn-2-en-7-one (NEO) mechanophores, we establish the relationship between these features and the force-dependent energetic changes along the reaction pathways. We show that the complex kinetic behavior of the tensioned bonds is generally and quantitatively predicted by a simple multivariate linear regression based on the two easily computed features with a straightforward workflow. These results demonstrate a general mechanistic framework for mechanochemical reactions under tensile force and provide a highly accessible tool for the large-scale computational screening in the design of mechanophores.

INTRODUCTION

Over the last century, chemists have mastered the ability to precisely connect pairs of carbon atoms for the synthesis of complex structures ranging from pharmaceuticals to polymeric materials. Less attention has been given to precision C–C bond disconnection. In the past two decades, although the carbon–carbon (C–C) bond is widely acknowledged for its strength, its scission is surprisingly common in a diverse array of selective mechanochemical transformations.[1–4] These transformations, which are the defining characteristic of mechanophores,[5,6] often exploit the homolytic activation of C–C bonds to achieve desired chemical[7–9] and physical changes.[10–12] Despite the number of mechanophores and computational tools for mechanochemical modeling,[3,13–15] due to the intricate coupling of force vectors and reaction trajectories,[16,17] examining C–C bond reactivity under tension typically requires extensive experimental efforts or electronic structure calculations with non-trivial transition state (TS) searches,[7,10,13,18–20] limiting the discovery of new mechanophores. We, therefore, sought a simple and predictive model of mechanochemical reactivity that connects state-of-the-art *ab initio* computations to concepts from the physical organic canon in a way that is immediately useful, intuitive to non-specialists, and provides a framework for further refinement.

RESULTS AND DISCUSSION

The tension-activated bond hypothesis

The classical Morse potential with its anharmonic shape motivates the concept of an effective force constant (k_{eff}) and reaction energy (ΔE) for mechanochemical transformations in polyatomic molecules where C–C bond scission is the rate-determining step (RDS). The Morse function describes the potential of diatomic molecules that

THE BIGGER PICTURE

Mechanical force has recently emerged as a unique stimulus to drive selective and productive C–C bond activations. However, the molecular details of force-to-chemical transduction are poorly captured by conventional chemical intuition due to its vectoral nature, making it challenging to understand and predict structure-reactivity relationships under tension. Here, we developed an intuitive physical organic model that captures C–C bond reactivities under tensile force by leveraging two molecular features: the effective force constant of the scissile bond (k_{eff}) and the force-free reaction energy (ΔE). A linear model was then established to accurately predict the transition force (f^*) required for C–C bond activation in over 30 mechanophores. This framework provides an intuitive mechanistic picture that facilitates the development of both new reactions under force and unprecedented mechanically responsive materials.

All rights are reserved, including those for text and data mining, AI training, and similar technologies.

have an equilibrium bond length of L_0 and bond dissociation energy U_0 (Figure 1A). The derivative of the Morse function with respect to interatomic displacement yields the restoring force curve that describes how strongly the pair of atoms are pulled toward L_0 for a given displacement, ΔL. The slope of the restoring force curve at L_0 is the Hookean force constant, k, which characterizes the bond's stiffness or resistance to deformation. The maximum value of the curve corresponds to f_{max}, and the area under the force curve corresponds to U_0. We introduce the restoring force triangle as a helpful mnemonic that approximates the restoring force curve (Figure 1A), characterized by its area ($\sim U_0$), front slope k, and back slope ($-k/8$), derived from the inflection point of the restoring force curve (Figure S1). In contrast to the simple uniaxial loading of force in diatomic molecules, the transfer of forces in polyatomic molecules becomes more intricate due to the influence of stereochemical and electronic features from substituents attached to carbon atoms (i.e., handles), known as the lever-arm effect.[16,17,21] To model force transmission from remote handles (Figures 1B and 1C), we introduce k_{eff}. We note that k_{eff} is not an intrinsic property of the scissile bond but a property that is highly dependent on the nature of handles and the directionality of applied force. Additionally, we replace the diatomic term U_0 with ΔE, representing the change in bond energy from the force-free ground-state (GS) to the diradical intermediate in polyatomic molecules (Figure 1B).

When a constant tension, f_0, is applied to the handles, the C–C bond stretches until the force is balanced by the molecule's internal restoring force (Figure 1B). A new minimum point is generated on the resulting force-modified potential energy surface (FMPES, blue dashed line),[22,23] which is named the tension-activated bond (TAB) (Figure 1C). The FMPES exhibits an activation barrier at the local maximum, which occurs at a specific bond displacement where the applied force intersects with the downward slope of the restoring force triangle (Figure S2). This position corresponds to the tensioned TS (TTS) for bond dissociation. Further deformation beyond the TTS leads to the formation of a tensioned diradical intermediate (TI) (Figures 1B and 1C). Notably, when f_0 equals f_{max}, the TAB and TTS converge to a single geometry, enabling the reaction to proceed through a barrierless process.

We use the restoring force triangle to qualitatively understand C–C bond reactivity under tension. For C–C bonds that have identical ΔE (same area under the triangle) but distinct k_{eff} values (e.g., *cis* vs. *trans* configuration) (Figure 1D), the one that exhibits a smaller k_{eff} corresponds to a more deformed TAB and a lower f_{max}, implying higher reactivity under tension (Figure 1D). Conversely, for a pair of molecules with handles of identical stereochemistry but differing in substituents that exert electronic influences on the C–C bond and/or the developing radical character, ΔE is anticipated to differ, whereas the k_{eff} values are nearly identical. In this scenario, the position of the TAB is unchanged, but the one with the smaller ΔE exhibits a lower f_{max} and an earlier TTS, indicating higher reactivity under f_0 (Figure 1E). Therefore, it is intuitive to expect that C–C bonds with lower resistance to deformation (i.e., smaller k_{eff}) or intrinsically more reactive (i.e., smaller ΔE) will display enhanced reactivity under tension. Based on these conjectures, we posit a physical organic model, termed the tension model of bond activation (TMBA), which captures the mechanochemical activation of C–C bonds in complex molecules using the two easily computed parameters: k_{eff} and ΔE.

We developed the TMBA from mechanistic studies on the norborn-2-en-7-one (NEO) mechanophores.[24] In our initial report of NEO mechanochemistry,[24] we proposed a unique stepwise activation mechanism involving two elementary steps, both of which include C–C bond cleavages (Figure 2A). The widely used computational tool CoGEF (constrained geometries simulate external force),[25,26] however,

[1]Department of Chemistry, University of Illinois at Urbana-Champaign, Urbana, IL 61801, USA

[2]Beckman Institute for Advanced Science and Technology, University of Illinois at Urbana-Champaign, Urbana, IL 61801, USA

[3]Department of Chemical Engineering, Massachusetts Institute of Technology, Cambridge, MA 02139, USA

[4]Department of Chemistry, Duke University, Durham, NC 27708, USA

[5]Department of Chemistry, Massachusetts Institute of Technology, Cambridge, MA 02139, USA

[6]These authors contributed equally

[7]Lead contact

*Correspondence: stephen.craig@duke.edu (S.L.C.), hjkulik@mit.edu (H.J.K.), jsmoore@illinois.edu (J.S.M.)

https://doi.org/10.1016/j.chempr.2024.05.012

Please cite this article in press as: Sun et al., The tension-activated carbon–carbon bond, Chem (2024), https://doi.org/10.1016/j.chempr.2024.05.012

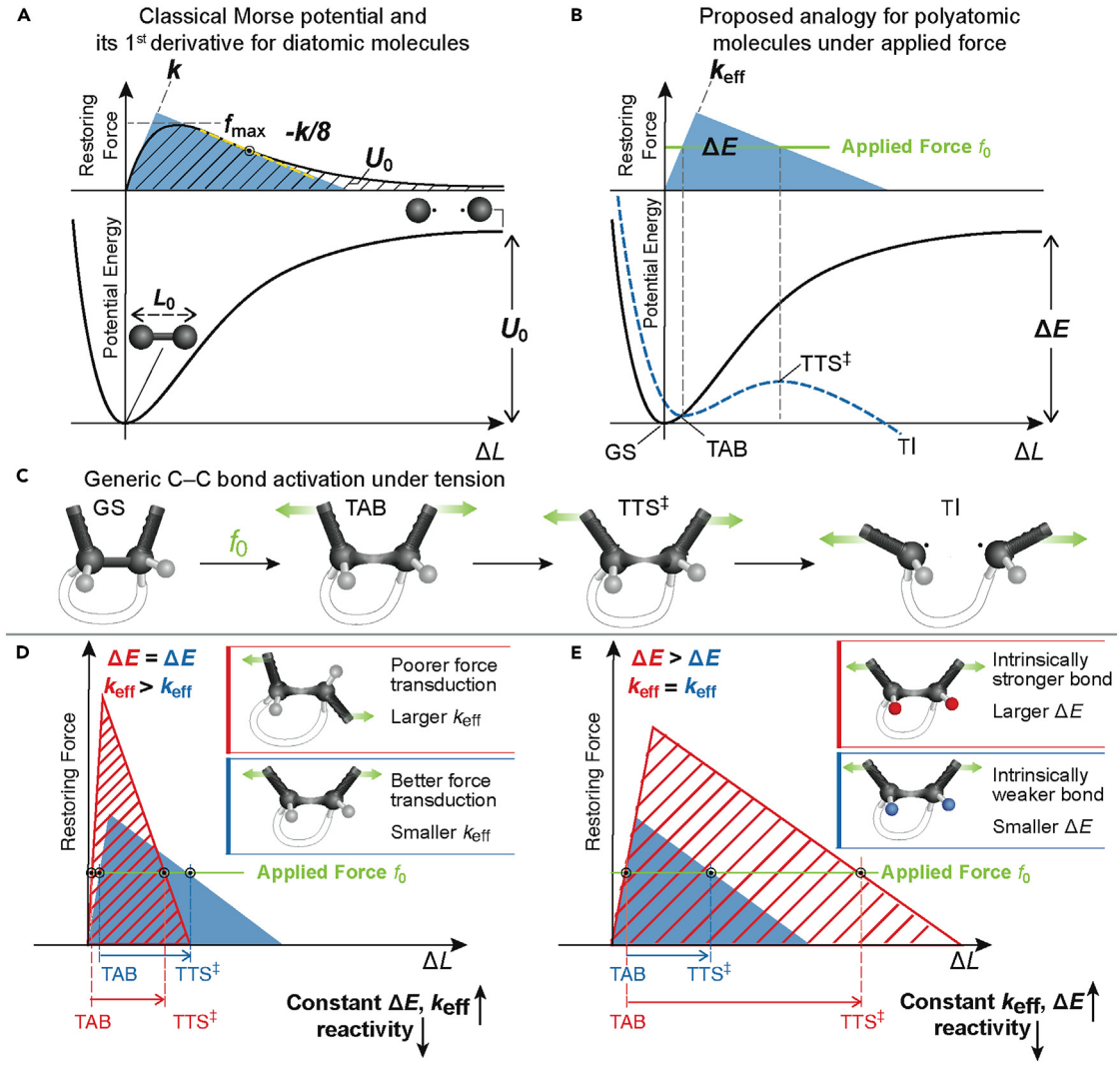

Figure 1. Schematic representation of the tension model of bond activation

(A) Illustration of the anharmonic Morse potential and its derivative for a diatomic molecule, depicting the relationship between the restoring force curve and the restoring force triangle.

(B) Representation of the force-modified potential energy surface (FMPES) profile for a polyatomic molecule under static tension (f_0) and its correspondence with the restoring force triangle.

(C) Schematic diagrams of the force-free ground state (GS), tension-activated bond (TAB), the tensioned transition state (TTS), and the tensioned intermediate (TI).

(D) Influence of the effective force constant (k_{eff}) on the position of TAB, TTS, and the maximum force (f_{max}) for C–C bonds with identical energy change (ΔE) but varying k_{eff} values.

(E) Influence of the energy change (ΔE) on the position of TAB, TTS, and f_{max} for C–C bonds with identical handle stereochemistry but different ΔE values resulting from electronic perturbations caused by the substituents.

failed to capture its critical aspects of the observed reactivity (Figure S3). We therefore initiated computational evaluations of isotensional activation energies using a rigorous method, leading to insights that began to frame the TMBA. We also synthesized two new NEO derivatives (alkyl-*endo* and alkyl-*exo*) with the previously reported acyl-*endo* and acyl-*trans* to generate a set of structures with diverse stereochemistry and substituents (Figure 2B) that impact k_{eff} and ΔE similar to the examples illustrated in Figures 1D and 1E. The physical organic insights gained from these mechanistic studies enabled us to refine and expand the qualitative

Please cite this article in press as: Sun et al., The tension-activated carbon–carbon bond, Chem (2024), https://doi.org/10.1016/j.chempr.2024.05.012

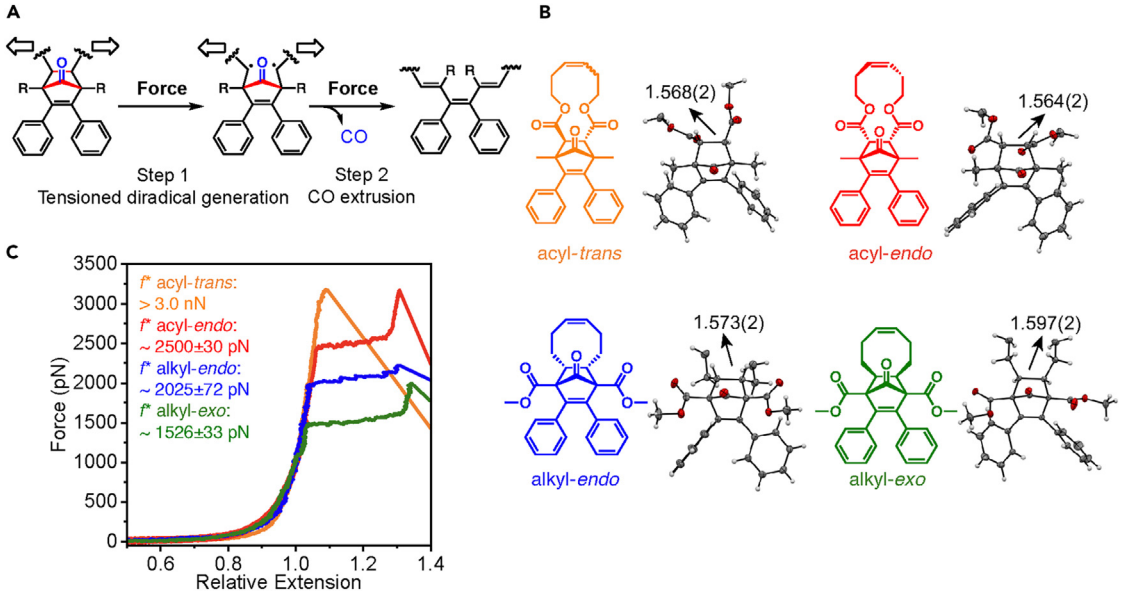

Figure 2. NEO mechanophore moieties and the experimental characterizations

(A) Postulated stepwise mechanism of CO-releasing NEO mechanophores.

(B) Chemical structures and corresponding single crystals of the four ROMP-able NEO derivatives. The lengths (Å) of the C–C bond cleaved in the diradical generation step are indicated, with the standard deviation in parentheses. The cycloalkene fragments are omitted for clarity.

(C) Representative single-molecule force curves of NEO copolymers obtained through SMFS.

TMBA into a parametric equation with broad applicability to predict mechanochemical C–C bond activation processes in numerous other mechanophores.

Distinct mechanochemical reactivities of four NEO derivatives

The four NEO derivatives depicted in Figure 2B demonstrate variations in both functional groups and stereochemistry of the handles. These differences allow us to explore the influence of steric, electronic, and conformational factors on the stability of both the GS and intermediate. The four NEO derivatives were incorporated in polymers using ring-opening metathesis polymerization (ROMP) and displayed distinct mechanochemical reactivities, as evidenced by ultrasonication and single-molecule force spectroscopy (SMFS) studies using an atomic force microscope.[27] In the ultrasonication experiments, all four derivatives exhibited mechanochemical activity when subjected to a pulsed acoustic field.[4,5] Competition studies ranked their relative mechanochemical reactivities as follows: *cis* > *trans*; *exo* > *endo*; and alkyl > acyl (Figure S12). The SMFS analysis provided quantitative data on the transition force (f^*) required for activation (Figure 2C).[19,28,29] Interestingly, the force-extension curve for the acyl-*trans* did not show a plateau prior to detachment, indicating an f^* beyond the measurable range (>3.0 nN). In contrast, all three *cis* derivatives displayed distinct plateau regions, each characterized by different f^* values. Specifically, the f^* values were approximately 2,500 ± 30, 2,025 ± 72, and 1,526 ± 33 pN for the respective *cis* derivatives (Figure 2C). The trends observed in SMFS are consistent with the mechanochemical reactivity observed in the ultrasonication experiments. The significant impact of subtle structural variations on f^* prompted an extensive computational investigation to gain a deeper understanding of the relationship between structure and reactivity within the framework of the TMBA.

Mechanistic investigation of NEO activation

The external force explicitly included (EFEI) method[30,31] enabled us to locate the TAB, TTS, and TI on the FMPES. We thus computed the isotensional activation

Please cite this article in press as: Sun et al., The tension-activated carbon–carbon bond, Chem (2024), https://doi.org/10.1016/j.chempr.2024.05.012

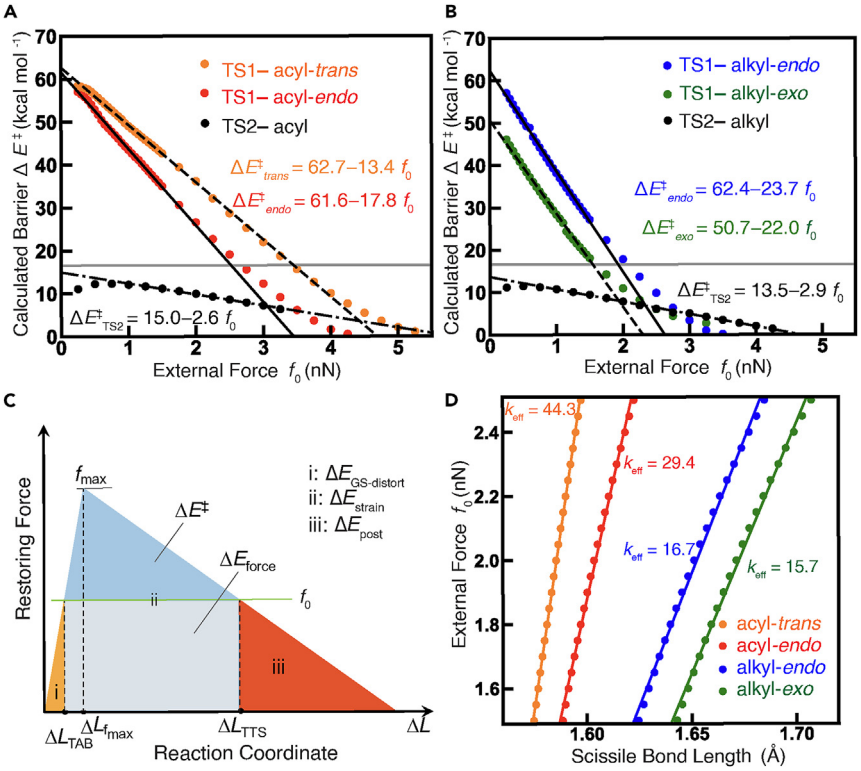

Figure 3. Electronic structure simulations on NEO derivatives and their connection to TMBA

(A and B) The EFEI-calculated activation energies for the four NEO mechanophores plotted against the applied force (f_0). The colored dots represent the $\Delta E^{\ddagger}$ corresponding to the first C–C bond cleavages. The black dots represent the $\Delta E^{\ddagger}$ corresponding to the CO extrusion step from the respective diradical intermediates. The horizontal gray lines indicate the threshold of $\Delta E^{\ddagger}$, below which rapid thermal activation is expected based on transition state theory at 298 K at the timescale of the SMFS experiment.

(C) The restoring force triangle is utilized to illustrate different segments of the reaction coordinate and the corresponding changes in electronic energy. The energy required for ground-state distortion (orange, segment i) and post-transition-state region (red, segment iii) is obtained through external mechanical force. The energy for the progression from TAB to TTS (blue triangle + gray rectangle, segment ii) is a combination of external mechanical work (ΔE_{force}) and external thermal energy ($\Delta E^{\ddagger}$).

(D) The computational data used to determine the effective stiffness (k_{eff}) for the four NEO mechanophores. The k_{eff} value quantifies the resistance of the bond to stretching when tension is applied remotely and transmitted through the handles to the scissile bond. The observed linear relationships provide support for the Hookean approximation of mechanophores in the vicinity of the GS.

energies, $\Delta E^{\ddagger}$s, for each NEO derivative from low (0.25 nN) to high (5.25 nN) external force values. The EFEI method successfully identified barriers associated with the TTSs for both steps of the proposed two-step sequence in Figure 2A. As noted previously and seen in the TMBA framework, the force required to lower $\Delta E^{\ddagger}$ to zero corresponds to f_{max}.[32] When the applied force is less than f_{max}, thermal energy becomes necessary in addition to the force to overcome the nonzero $\Delta E^{\ddagger}$ barrier. Because the EFEI calculations determine $\Delta E^{\ddagger}$ at each f_0 value, the reaction kinetics at a specific f_0 and temperature can be predicted using TS theory.

To examine the accuracy of EFEI simulations for NEOs, we compared the predicted f^* with experimental SMFS studies. The f^* in SMFS reflects the force at which the chain extension rate is comparable with that of the mechanochemical reaction, which typically involves reaction half-lives of ~0.1 s.[21,33] The corresponding $\Delta E^{\ddagger}$ for each mechanophore is ~16.0 kcal·mol^{-1} at 298 K (Figure S79), as represented by the gray line in Figures 3A and 3B. Therefore, the calculated values of f^* were obtained from the points of intersection between the horizontal line and $\Delta E^{\ddagger}$. The predicted values of f^* are approximately 3.4, 2.6, 2.0, and 1.6 nN for acyl-*trans*,

Please cite this article in press as: Sun et al., The tension-activated carbon–carbon bond, Chem (2024), https://doi.org/10.1016/j.chempr.2024.05.012

acyl-*endo*, alkyl-*endo*, and alkyl-*exo* correspondingly, indicating a good agreement between simulation and experiments.

Qualitative mechanistic insight was gained from the force dependence of $\Delta E^{\ddagger}$s shown in Figures 3A and 3B. The $\Delta E^{\ddagger}$ of the initial C–C bond scission exhibits a monotonic decrease as f_0 increases. In contrast, the energy landscape for the CO-releasing step (indicated by black dots) appears relatively flat, particularly in the low force region. The EFEI computed values of $\Delta E^{\ddagger}$ for the CO-releasing step are below the thermal threshold (gray line) for all values of f_0. This implies that the CO-releasing step proceeds spontaneously and rapidly during SMFS once the diradical intermediate is formed. In contrast, the $\Delta E^{\ddagger}$ for the initial C–C bond scission is significantly higher than the thermal threshold in the low force region but rapidly approaches the threshold with increasing f_0. Furthermore, although the $\Delta E^{\ddagger}$ of the first step experiences a more rapid change, it consistently remains higher than that of the CO-releasing step across the low force range (<3 nN) for all NEO variants. This computational result suggests diradical generation as the RDS under typical experimental force conditions.

The plots presented in Figures 3A and 3B highlight quantitative aspects of the relationship between structure and reactivity of C–C bonds under tension. These plots exhibit a linear relationship in the low to intermediate force range (0.25–1.5 nN).[21] The slope and intercept obtained from linear regression analysis hold significant implications in the context of the TMBA. First, the force-free activation energy ($\Delta E^{\ddagger}|_{f=0}$) represents the inherent reactivity of the mechanophore. Figures 3A and 3B show that the *trans* derivative and the two *endo* derivatives have similar $\Delta E^{\ddagger}|_{f=0}$ values of approximately 62 kcal•mol^{-1} for the first C–C bond scission. In contrast, the *exo* isomer exhibits a significantly lower $\Delta E^{\ddagger}|_{f=0}$ value of approximately 51 kcal•mol^{-1}. This lower $\Delta E^{\ddagger}|_{f=0}$ value indicates an enhanced inherent reactivity of the alkyl-*exo* compared with the other derivatives. Indeed, an elongated C–C bond in the alkyl-*exo* derivative is observed in single-crystal structures (Figure 2B). The slopes of the linear regressions reveal the sensitivity of the mechanophore's reactivity to applied tension and correspond to the mechanochemical coupling constant (γ).[21] From Figures 3A and 3B, it can be observed that the *cis* configurations are more responsive to tension compared with the *trans* configuration, which is consistent with observations made for other mechanophores.[29,34] Therefore, the higher reactivity of the acyl-*endo* relative to the acyl-*trans* under tension is attributed to mechanochemical coupling effects rather than inherent reactivity differences. Also, the alkyl handles lead to enhanced mechanochemical coupling compared with acyl handles, resulting in the higher reactivity of the alkyl-*endo* relative to the acyl-*endo*.

Development of the quantitative TMBA

Analyzing the EFEI calculations at various stages along the reaction pathway, including the transition from the force-free GS to the TAB, from the TAB to the TTS, and the post-TTS segment, provides insights into the influence of tension on energetic changes and tension-induced distortions and helps elucidate the molecular features that govern the observed differential reactivity among the NEO derivatives within the TMBA framework (Figure S23). When molecular distortions occur from the GS to ΔL_{TAB}, there is an associated increase in electronic energy, referred to as $\Delta E_{GS\text{-}distort}$, represented by area i on the restoring force triangle (Figure 3C). As the C–C bond extends from position ΔL_{TAB} to ΔL_{TTS}, the electronic energy further increases, as indicated by area ii. Finally, the electronic energy change accompanying the post-TTS region (ΔE_{post}) of the reaction coordinate is represented by area iii. The total area enclosed within the restoring force triangle, ΔE, encompasses the sum of all electronic energies represented by areas i, ii, and iii. In progressing

Please cite this article in press as: Sun et al., The tension-activated carbon–carbon bond, Chem (2024), https://doi.org/10.1016/j.chempr.2024.05.012

from ΔL_{TAB} to ΔL_{TTS}, external mechanical work contributes energy (ΔE_{force}, bottom rectangular area) equivalent to $-f_0 \times (\Delta L_{TTS} - \Delta L_{TAB})$, effectively reducing the barrier height to $\Delta E^{\ddagger}$ = ii + ΔE_{force} (where ΔE_{force} is a negative value). Thermal energy ($\Delta E^{\ddagger}$, top triangular area) assists to overcome this barrier.[25] Thus, under tension, mechanical work fully contributes the energies associated with the initial and final distortions along the reaction coordinate, specifically areas i and iii. Area ii is supplied by a combination of mechanical work and thermal energy. As visualized by the restoring force triangle, as f_0 increases, the positions of ΔL_{TTS} and ΔL_{TAB} move closer together, ultimately converging at ΔL_{fmax} when f_0 reaches f_{max}. As a result, area ii decreases from a value of ΔE at f_0 = 0 to a value of zero at $f_0 = f_{max}$.

Next, we utilized this segmentation to analyze the EFEI calculations of the four NEO derivatives. Drawing inspiration from the activation strain model, which has proven successful in elucidating the reactivity of various thermal reactions,[35,36] we defined ΔE_{strain} as the energy difference between positions ΔL_{TTS} and ΔL_{TAB}, as determined by the EFEI calculations. This energy change is visually represented as area ii in Figure 3C. We investigated the EFEI-calculated dependence of ΔE_{strain} and ΔE_{force} on f_0 within the range of 0.25 to 2.50 nN for the four NEO derivatives. In the force regions of 1.5–2.5 nN where experimental scission was observed, the four NEO variants exhibited distinct ΔE_{strain} values, differing by up to 30 kcal·mol^{-1} (Figure S24). Importantly, these ΔE_{strain} trends align with the experimental reactivities ranking the structural features according to ΔE_{strain} as follows: *exo* < *endo*; alkyl < acyl; *cis* < *trans*. In contrast, the variations in ΔE_{force} among the four NEO derivatives are less profound (Figure S24), and the ΔE_{force} values do not correlate with experimental reactivities.

In considering how the structural features influenced $\Delta E_{GS\text{-}distort}$ and ΔE_{post} (areas i and iii), we analyzed the scissile C–C bond length in both the TAB and TTS structures as a function of f_0. Interestingly, the four NEO variants exhibit distinct distortions at ΔL_{TAB}, with the alkyl-*exo* derivative showing the greatest stretching, followed by the alkyl-*endo* and then the acyl derivatives. By comparison, the acyl-*trans* derivative exhibits the least distortion (Figure S24). The f_0-dependent distortions at ΔL_{TTS} are more similar among the NEO variants until approximately 2.0 nN. These results suggest that $\Delta E_{GS\text{-}distort}$ plays a more significant role than ΔE_{post} in influencing mechanochemical reactivity. Thus, we conclude that the distinct γ values of NEOs are mainly contributed by differing $\Delta E_{GS\text{-}distort}$ with some contributions from ΔE_{force}.

The full EFEI mechanistic investigations involving TS searches under tension can be computationally intensive, rendering them impractical for the iterative design and accelerated discovery of new mechanophores. We posit that the TMBA offers a framework for developing a more accessible yet still predictive parametric calculation of mechanophore reactivity. In practical terms, we sought to correlate k_{eff} and ΔE in the TMBA with the slope (γ) and intercept (force-free $\Delta E^{\ddagger}$) observed in the linear correlations shown in Figures 3A and 3B. We first reasoned that mechanophores can be treated as Hookean objects, responding to force with an extent of GS distortion described by k_{eff}. For instance, C–C bonds with higher resistance to deformation (larger k_{eff}) will exhibit a smaller $\Delta E_{GS\text{-}distort}$ for a given f_0, as conceptualized in Figure 1D (Figure S32). The stiffness constant is hypothesized as an alternative for $\Delta E_{GS\text{-}distort}$ that reflects how deformation depends on force. Consistent with Hammond's postulate,[37] ΔE for the formation of the diradical intermediate estimates the relative extension in the TS (as conceptualized in Figure 1E). Because ΔE_{force} is controlled by the displacement between TAB and TTS ($\Delta L_{TTS} - \Delta L_{TAB}$) at a certain f_0, we reason that ΔE correlates with ΔE_{force}. For instance, a late TS (large $\Delta L_{TTS} - \Delta L_{TAB}$) is expected for C–C bonds that are intrinsically more stable (larger ΔE) and

Please cite this article in press as: Sun et al., The tension-activated carbon–carbon bond, Chem (2024), https://doi.org/10.1016/j.chempr.2024.05.012

have more negative ΔE_{force} (Figure S33). Moreover, we envisioned that ΔE approximates the force-free $\Delta E^{\ddagger}$ based on the Bell-Evans-Polanyi principle.[38] Therefore, both the slope and the intercept in Figures 3A and 3B are envisioned to correlate with ΔE and k_{eff}, suggesting the possibility of directly predicting the force required to reach a certain $\Delta E^{\ddagger}$ with only these two parameters. We chose the prediction of f^* exhibited in SMFS studies as the target where the mechanophore reactivity corresponds to force-coupled activation barriers of ~16–17 kcal•mol^{-1}.[21,29,33]

To assess the Hookean spring-like behavior of the scissile C–C bond near the GS, a computational force was incrementally applied through the handles in 0.05 nN intervals within the range of 1.5–2.5 nN, and the molecules were optimized to the resulting TAB. A linear correlation between the f_0 and C–C bond length was observed for all four NEO variants. The slope provided the constant k_{eff}, which was determined to be 29.4, 44.3, 16.7, and 15.7 nN Å^{-1} for acyl-*endo*, acyl-*trans*, alkyl-*endo*, and alkyl-*exo*, respectively (Figure 3D). This Hookean-like behavior was found to be a general feature for an additional 27 mechanophores with known f^* in SMFS, encompassing cyclopropane, cyclobutane, and cyclobutene moieties (Figures S34–S36).

To predict the experimental f^* for C–C bond activation events, we computed the ΔE values for a total of 31 mechanophores that have been tested in SMFS. For mechanophore **1–24**, ΔE were calculated using the same procedure without explicit adjustments based on accepted mechanistic factors other than homolytic scission (Figure 4A). Intriguingly, partial halogen dissociation was observed during the geometry optimization of the gem-dibromocyclopropane (gDBC) and gem-dichlorocyclopropane (gDCC) mechanophores. Given that gDBCs and gDCCs are believed to undergo ring opening through a concerted pathway, these compounds were retained in model training because the optimized geometries are in agreement with the previously proposed mechanism.[39,40] Using a multivariate linear regression model, we investigated the relationship between the f^* and the two key parameters, k_{eff} and ΔE. Remarkably, we found that employing these two parameters for multivariate linear regression can predict f^* for 23 mechanophores with high accuracy including NEO, cyclopropane, ladderane, and cyclobutane moieties. The resulting model demonstrated a mean absolute error (MAE) of 0.17 nN and an R^2 value of 0.88, indicating a strong correlation between the predicted and experimental f^* values (Figure 4A). Several additional cross-validation tests confirmed the robustness of the model. However, we noted that this predictive model did not accurately capture the behavior of seven cyclobutene mechanophores (Figure S37). Because these seven cyclobutenes may follow a 4π electrocyclic ring-opening mechanism that involves additional secondary orbital interactions, this might lead to off-scale ΔE energies, making the generalization of the model to cyclobutene mechanophores challenging. We performed a separate linear regression on the cyclobutene mechanophores showing improved accuracy (Figure S38). These findings suggest that although the coefficients in the TMBA may vary depending on the specific mechanophore activation mechanism, the general predictive framework based on k_{eff} and ΔE remains valid. Because the modeled handle length is known to potentially impact the mechanochemical transduction,[32] we investigated its effects on reaction kinetics and k_{eff} values for NEO mechanophores. Only minimal differences were observed in our case, suggesting the robustness of the TMBA (Figures S39 and S40).

The TMBA approach offers several advantages, including its high computational efficiency by circumventing TS searches and enabling parallelization of several isotensional optimizations that are not possible with CoGEF, which requires several serial optimization steps. Furthermore, although k_{eff} was computed using 21 isotensional geometries

Please cite this article in press as: Sun et al., The tension-activated carbon–carbon bond, Chem (2024), https://doi.org/10.1016/j.chempr.2024.05.012

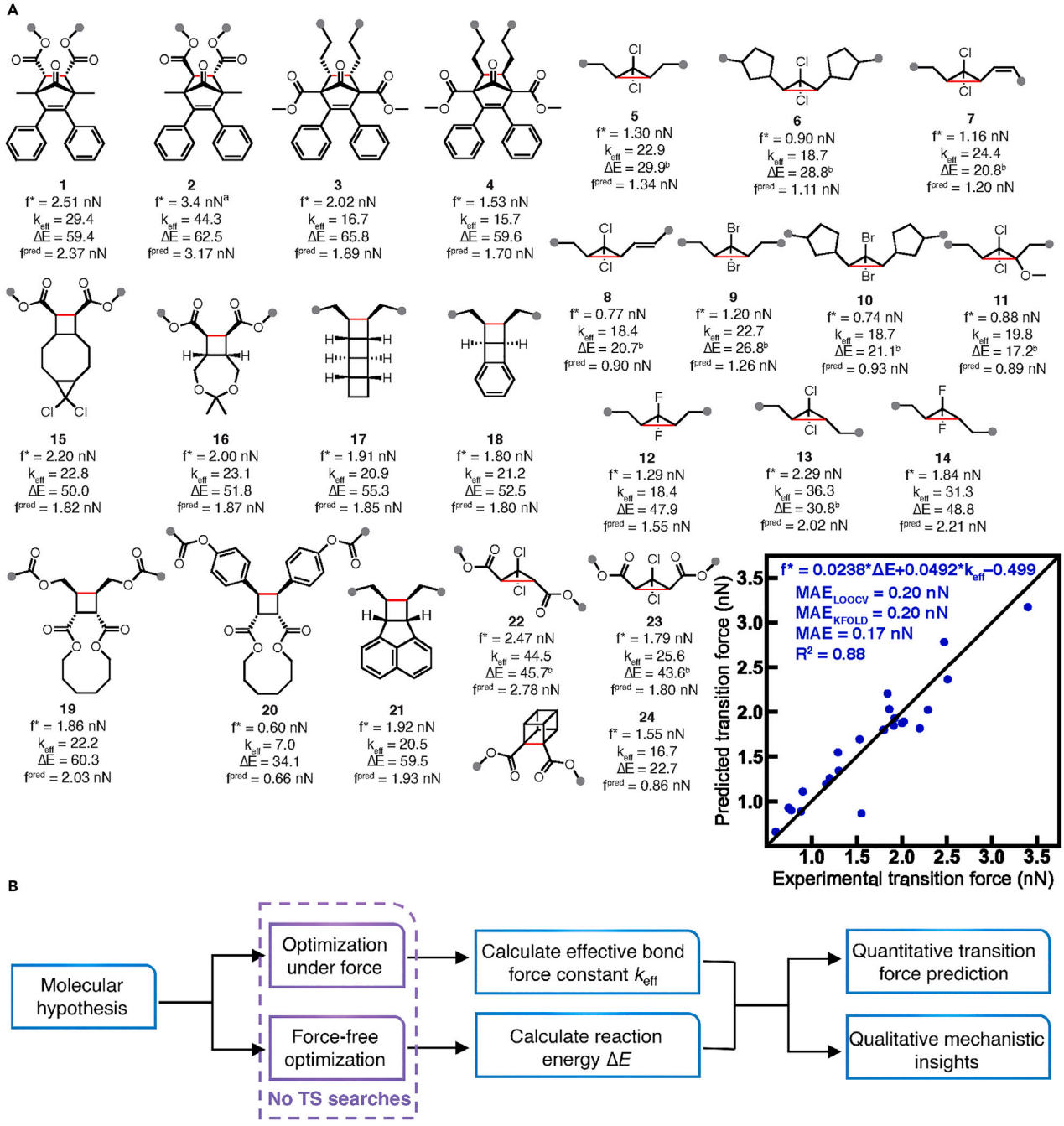

Figure 4. The linear model for predicting reactivity under force

(A) Multivariate linear regression model for the prediction of experimental transition forces (*f**). The chemical structures depict the experimental *f** measured on polymeric samples in SMFS and calculated parameters used in the trained model. The gray circles represent the atoms to which external force is applied. MAE_{LOOCV} represents the mean absolute error obtained from leave-one-out cross-validation (LOOCV), where each mechanophore serves as the test set, whereas the remaining mechanophores are used for multivariate regression. MAE_{KFOLD} refers to the average MAE from repeated k-fold cross-validation with 80:20 train/test splits and 100 randomized splits. [a]Note that for acyl-*trans*, the simulated *f** from EFEI calculations was utilized due to the absence of experimental SMFS data. [b]The ΔE values are calculated from intermediates with partial halide dissociation.

(B) Workflow illustrating the application of the model to mechanophores in this work and potentially other mechanophores. We note that the calculation of k_{eff} requires 3 to 21 optimizations under force. The calculation of ΔE requires two force-free optimizations and two single-point energy simulations. Procedures that require DFT simulations are highlighted in purple.

Please cite this article in press as: Sun et al., The tension-activated carbon–carbon bond, Chem (2024), https://doi.org/10.1016/j.chempr.2024.05.012

in Figure 4A, we found that three geometries are sufficient to model k_{eff} accurately, indicating the further improved efficiency of TMBA (Figure S42). It also shows improved performance to predict mechanochemical reactivities across different mechanophores compared with CoGEF (Figures S74 and S75). Most importantly, it provides immediate insights into structure-reactivity trends that significantly enhance the chemical intuition in mechanochemistry, where lower k_{eff} values indicate improved mechanochemical coupling and lower ΔE values suggest more favorable intrinsic reactivity. For example, mechanophores **6** and **10** have identical k_{eff} values but different ΔE values, indicating that the lower f^* of mechanophore **10** is primarily influenced by thermodynamic effects (Figure 4A). Similarly, mechanophore **6** exhibits similar ΔE but a smaller k_{eff} compared with mechanophore **5**, suggesting enhanced mechanochemical coupling due to the presence of cyclopentenyl handles, consistent with previous studies.[16] Moreover, replacing alkyl handles with aryl handles in mechanophore **19** results in improved coupling and more favorable intrinsic activation, leading to a significant decrease in the f^* observed in **20**.[41] A straightforward computational workflow is depicted in Figure 4B and a detailed tutorial can be found in the supplemental information.

Conclusions

Although the Morse potential has been utilized as the very first mechanochemistry model[22,42] and the restoring force plot has been proposed to understand bond activation upon stretching,[23,43] the current work identifies two key molecular features (i.e., k_{eff} and ΔE) that capture the behaviors of bonds under external force from these known models. We then took advantage of the unique NEO platform, where a wide range of mechanochemical reactivities were accessed using a series of derivatives with high structural homology to further extend the qualitative analysis to the quantitative prediction of the C–C bond mechanochemical activation process.

From our results, the complex kinetic behavior of tensioned bonds can be reduced to two simple parameters across various C–C activation mechanophores that have distinct core structures. We note that, although the f^* in SMFS was chosen in this work to fairly compare different mechanophores with experimental data, the multivariate linear regression in TMBA presumably applies to force values that correspond to other kinetic regions. We envision that the TMBA can be generalized to other mechanochemical bond scission processes beyond C–C activation. Specifically, qualitative physical organic insights can be obtained by simply calculating k_{eff} and ΔE values for computational screening of new mechanophores.[44] Quantitative f^* value prediction can be performed by establishing the linear regression when having a series of experimental data or comprehensive electronic simulation results (e.g., EFEI) available. The simplicity and accessibility of TMBA will facilitate the discovery of new mechanophores and enhance our understanding of structure-reactivity relationships, leading to advancements in the field of mechanochemistry.

EXPERIMENTAL PROCEDURES

Resource availability

Lead contact

Further information and requests for additional details should be directed to and will be fulfilled by the lead contact, Jeffrey S. Moore (jsmoore@illinois.edu).

Materials availability

This study did not generate new unique reagents. Crystallographic data are available free of charge from the Cambridge Crystallographic Data Centre under reference CCDC nos. 2278660 and 2278661. All other data are available in the main text or the supplemental information.

Please cite this article in press as: Sun et al., The tension-activated carbon–carbon bond, Chem (2024), https://doi.org/10.1016/j.chempr.2024.05.012

CellPress

Data and code availability

All of the data supporting the findings of this study are presented within the article and supplemental information. All other data are available from the lead contact upon reasonable request.

SUPPLEMENTAL INFORMATION

Supplemental information can be found online at https://doi.org/10.1016/j.chempr.2024.05.012.

ACKNOWLEDGMENTS

We thank Shu Wang for the discussion on Morse potential and its derivatives, Dorothy Loudermilk for figure designs, and Toby Woods for X-ray crystallography help. This work was supported by the NSF Center for the Chemistry of Molecularly Optimized Networks (MONET), CHE-2116298. This work used Expanse at San Diego Supercomputing Center through allocation CHE140073 from the Advanced Cyberinfrastructure Coordination Ecosystem: Services and Support (ACCESS) program, which is supported by National Science Foundation grants #2138259, #2138286, #2138307, #2137603, and #2138296.

AUTHOR CONTRIBUTIONS

Y.S. and I.K. contributed equally to this work. Y.S., I.K., and J.S.M. conceived the idea. Y.S. conducted synthetic experiments, solution ultrasonication, and some of the density functional theory (DFT) simulations. I.K. conducted most of the DFT calculations and the linear regression. Z.P.B. performed some of the monomer synthesis. T.B.K. conducted the single-molecule force spectroscopy measurement. S.L.C., H.J.K., and J.S.M. supervised the project. Y.S. and I.K. wrote the original manuscript and all authors participated in the review and editing.

DECLARATION OF INTERESTS

Heather Kulik serves as a member of the advisory board of *Chem*.

Received: January 22, 2024
Revised: March 4, 2024
Accepted: May 20, 2024
Published: June 13, 2024

REFERENCES

1. Hickenboth, C.R., Moore, J.S., White, S.R., Sottos, N.R., Baudry, J., and Wilson, S.R. (2007). Biasing reaction pathways with mechanical force. Nature *446*, 423–427. https://doi.org/10.1038/nature05681.

2. Lenhardt, J.M., Ong, M.T., Choe, R., Evenhuis, C.R., Martinez, T.J., and Craig, S.L. (2010). Trapping a diradical transition state by mechanochemical polymer extension. Science *329*, 1057–1060. https://doi.org/10.1126/science.1193412.

3. Chen, Y., Mellot, G., Van Luijk, D., Creton, C., and Sijbesma, R.P. (2021). Mechanochemical tools for polymer materials. Chem. Soc. Rev. *50*, 4100–4140. https://doi.org/10.1039/d0cs00940g.

4. Caruso, M.M., Davis, D.A., Shen, Q., Odom, S.A., Sottos, N.R., White, S.R., and Moore, J.S. (2009). Mechanically-induced chemical changes in polymeric materials. Chem. Rev. *109*, 5755–5798. https://doi.org/10.1021/cr9001353.

5. Li, J., Nagamani, C., and Moore, J.S. (2015). Polymer Mechanochemistry: From Destructive to Productive. Acc. Chem. Res. *48*, 2181–2190. https://doi.org/10.1021/acs.accounts.5b00184.

6. De Bo, G. (2020). Polymer mechanochemistry and the emergence of the mechanophore concept. Macromolecules *53*, 7615–7617. https://doi.org/10.1021/acs.macromol.0c01683.

7. Nixon, R., and De Bo, G. (2020). Three concomitant C–C dissociation pathways during the mechanical activation of an N-heterocyclic carbene precursor. Nat. Chem. *12*, 826–831. https://doi.org/10.1038/s41557-020-0509-1.

8. Liu, Y., Holm, S., Meisner, J., Jia, Y., Wu, Q., Woods, T.J., Martinez, T.J., and Moore, J.S. (2021). Flyby reaction trajectories: Chemical dynamics under extrinsic force. Science *373*, 208–212. https://doi.org/10.1126/science.abi7609.

9. Chen, Y., Spiering, A.J.H., Karthikeyan, S., Peters, G.W.M., Meijer, E.W., and Sijbesma, R.P. (2012). Mechanically induced chemiluminescence from polymers incorporating a 1,2-dioxetane unit in the main chain. Nat. Chem. *4*, 559–562. https://doi.org/10.1038/nchem.1358.

10. Chen, Z., Mercer, J.A.M., Zhu, X., Romaniuk, J.A.H., Pfattner, R., Cegelski, L., Martinez, T.J., Burns, N.Z., and Xia, Y. (2017). Mechanochemical unzipping of insulating polyladderene to semiconducting polyacetylene. Science *357*, 475–479. https://doi.org/10.1126/science.aan2797.

11. Wang, Z., Zheng, X., Ouchi, T., Kouznetsova, T.B., Beech, H.K., Av-Ron, S., Matsuda, T.,

Please cite this article in press as: Sun et al., The tension-activated carbon–carbon bond, Chem (2024), https://doi.org/10.1016/j.chempr.2024.05.012

Bowser, B.H., Wang, S., Johnson, J.A., et al. (2021). Toughening hydrogels through force-triggered chemical reactions that lengthen polymer strands. Science *374*, 193–196. https://doi.org/10.1126/science.abg2689.

12. Wang, S., Hu, Y., Kouznetsova, T.B., Sapir, L., Chen, D., Herzog-Arbeitman, A., Johnson, J.A., Rubinstein, M., and Craig, S.L. (2023). Facile mechanochemical cycloreversion of polymer cross-linkers enhances tear resistance. Science *380*, 1248–1252. https://doi.org/10.1126/science.adg3229.

13. Ribas-Arino, J., and Marx, D. (2012). Covalent mechanochemistry: theoretical concepts and computational tools with applications to molecular nanomechanics. Chem. Rev. *112*, 5412–5487. https://doi.org/10.1021/cr200399q.

14. Stauch, T., and Dreuw, A. (2016). Advances in Quantum Mechanochemistry: Electronic Structure Methods and Force Analysis. Chem. Rev. *116*, 14137–14180. https://doi.org/10.1021/acs.chemrev.6b00458.

15. Bell, G.I. (1978). Models for the specific adhesion of cells to cells. Science *200*, 618–627. https://doi.org/10.1126/science.347575.

16. Klukovich, H.M., Kouznetsova, T.B., Kean, Z.S., Lenhardt, J.M., and Craig, S.L. (2013). A backbone lever-arm effect enhances polymer mechanochemistry. Nat. Chem. *5*, 110–114. https://doi.org/10.1038/nchem.1540.

17. Wang, J., Kouznetsova, T.B., Kean, Z.S., Fan, L., Mar, B.D., Martínez, T.J., and Craig, S.L. (2014). A remote stereochemical lever arm effect in polymer mechanochemistry. J. Am. Chem. Soc. *136*, 15162–15165. https://doi.org/10.1021/ja509585g.

18. Chen, Z., Zhu, X., Yang, J., Mercer, J.A.M., Burns, N.Z., Martinez, T.J., and Xia, Y. (2020). The cascade unzipping of ladderane reveals dynamic effects in mechanochemistry. Nat. Chem. *12*, 302–309. https://doi.org/10.1038/s41557-019-0396-5.

19. Horst, M., Yang, J., Meisner, J., Kouznetsova, T.B., Martínez, T.J., Craig, S.L., and Xia, Y. (2021). Understanding the Mechanochemistry of Ladder-Type Cyclobutane Mechanophores by Single Molecule Force Spectroscopy. J. Am. Chem. Soc. *143*, 12328–12334. https://doi.org/10.1021/jacs.1c05857.

20. Stevenson, R., and De Bo, G. (2017). Controlling reactivity by geometry in retro-Diels-Alder reactions under tension. J. Am. Chem. Soc. *139*, 16768–16771. https://doi.org/10.1021/jacs.7b08895.

21. Brown, C.L., Bowser, B.H., Meisner, J., Kouznetsova, T.B., Seritan, S., Martinez, T.J., and Craig, S.L. (2021). Substituent effects in mechanochemical allowed and forbidden cyclobutene ring-opening reactions. J. Am. Chem. Soc. *143*, 3846–3855. https://doi.org/10.1021/jacs.0c12088.

22. Kauzmann, W., and Eyring, H. (1940). The viscous flow of large molecules. J. Am. Chem. Soc. *62*, 3113–3125. https://doi.org/10.1021/ja01868a059.

23. Odell, J.A., Muller, A.J., Narh, K.A., and Keller, A. (1990). Degradation of Polymer Solutions in Extensional Flows. Macromolecules *23*, 3092–3103. https://doi.org/10.1021/ma00214a011.

24. Sun, Y., Neary, W.J., Burke, Z.P., Qian, H., Zhu, L., and Moore, J.S. (2022). Mechanically triggered carbon monoxide release with turn-on aggregation-induced emission. J. Am. Chem. Soc. *144*, 1125–1129. https://doi.org/10.1021/jacs.1c12108.

25. Beyer, M.K. (2000). The mechanical strength of a covalent bond calculated by density functional theory. J. Chem. Phys. *112*, 7307–7312. https://doi.org/10.1063/1.481330.

26. Klein, I.M., Husic, C.C., Kovács, D.P., Choquette, N.J., and Robb, M.J. (2020). Validation of the CoGEF method as a predictive tool for polymer mechanochemistry. J. Am. Chem. Soc. *142*, 16364–16381. https://doi.org/10.1021/jacs.0c06868.

27. Binnig, G., Quate, C.F., and Gerber, C. (1986). Atomic force microscope. Phys. Rev. Lett. *56*, 930–933. https://doi.org/10.1103/PhysRevLett.56.930.

28. Zhang, Y., Wang, Z., Kouznetsova, T.B., Sha, Y., Xu, E., Shannahan, L., Fermen-Coker, M., Lin, Y., Tang, C., and Craig, S.L. (2021). Distal conformational locks on ferrocene mechanophores guide reaction pathways for increased mechanochemical reactivity. Nat. Chem. *13*, 56–62. https://doi.org/10.1038/s41557-020-00600-2.

29. Wang, J., Kouznetsova, T.B., Niu, Z., Ong, M.T., Klukovich, H.M., Rheingold, A.L., Martinez, T.J., and Craig, S.L. (2015). Inducing and quantifying forbidden reactivity with single-molecule polymer mechanochemistry. Nat. Chem. *7*, 323–327. https://doi.org/10.1038/nchem.2185.

30. Ong, M.T., Leiding, J., Tao, H., Virshup, A.M., and Martínez, T.J. (2009). First principles dynamics and minimum energy pathways for mechanochemical ring opening of cyclobutene. J. Am. Chem. Soc. *131*, 6377–6379. https://doi.org/10.1021/ja8095834.

31. Ribas-Arino, J., Shiga, M., and Marx, D. (2009). Understanding covalent mechanochemistry. Angew. Chem. Int. Ed. Engl. *48*, 4190–4193. https://doi.org/10.1002/anie.200900673.

32. Ribas-Arino, J., Shiga, M., and Marx, D. (2010). Mechanochemical transduction of externally applied forces to mechanophores. J. Am. Chem. Soc. *132*, 10609–10614. https://doi.org/10.1021/ja104958e.

33. Akbulatov, S., and Boulatov, R. (2017). Experimental Polymer Mechanochemistry and its Interpretational Frameworks. ChemPhysChem *18*, 1422–1450. https://doi.org/10.1002/cphc.201601354.

34. Kryger, M.J., Munaretto, A.M., and Moore, J.S. (2011). Structure-mechanochemical activity relationships for cyclobutane mechanophores. J. Am. Chem. Soc. *133*, 18992–18998. https://doi.org/10.1021/ja2086728.

35. Bickelhaupt, F.M., and Houk, K.N. (2017). Analyzing reaction rates with the distortion/interaction-activation strain model. Angew. Chem. Int. Ed. Engl. *56*, 10070–10086. https://doi.org/10.1002/anie.201701486.

36. Bickelhaupt, F.M. (1999). Understanding reactivity with Kohn-Sham molecular orbital theory: E2-SN2 mechanistic spectrum and other concepts. J. Comput. Chem. *20*, 114–128. https://doi.org/10.1002/(SICI)1096-987X(19990115)20:1<114::AID-JCC12>3.0.CO;2-L.

37. Hammond, G.S. (1955). A correlation of reaction rates. J. Am. Chem. Soc. *77*, 334–338. https://doi.org/10.1021/ja01607a027.

38. Evans, M.G., and Polanyi, M. (1938). Inertia and driving force of chemical reactions. Trans. Faraday Soc. *34*, 11–24. https://doi.org/10.1039/tf9383400011.

39. Lenhardt, J.M., Black, A.L., and Craig, S.L. (2009). Gem-Dichlorocyclopropanes as abundant and efficient mechanophores in polybutadiene copolymers under mechanical stress. J. Am. Chem. Soc. *131*, 10818–10819. https://doi.org/10.1021/ja9036548.

40. Wu, D., Lenhardt, J.M., Black, A.L., Akhremitchev, B.B., and Craig, S.L. (2010). Molecular stress relief through a force-induced irreversible extension in polymer contour length. J. Am. Chem. Soc. *132*, 15936–15938. https://doi.org/10.1021/ja108429h.

41. Bowser, B.H., Wang, S., Kouznetsova, T.B., Beech, H.K., Olsen, B.D., Rubinstein, M., and Craig, S.L. (2021). Single-Event Spectroscopy and Unravelling Kinetics of Covalent Domains Based on Cyclobutane Mechanophores. J. Am. Chem. Soc. *143*, 5269–5276. https://doi.org/10.1021/jacs.1c02149.

42. Crist, B., Oddershede, J., Sabin, J.R., Perram, J.W., and Ratner, M.A. (1984). Polymer fracture - A simple model for chain scission. J. Polym. Sci. Polym. Phys. Ed. *22*, 881–897. https://doi.org/10.1002/pol.1984.180220510.

43. De Boer, J.H. (1936). The influence of van der Waals' forces and primary bonds on binding energy, strength and orientation, with special reference to some artificial resins. Trans. Faraday Soc. *32*, 10–37. https://doi.org/10.1039/tf9363200010.

44. Horst, M., Meisner, J., Yang, J., Kouznetsova, T.B., Craig, S.L., Martínez, T.J., and Xia, Y. (2024). Mechanochemistry of Pterodactylane. J. Am. Chem. Soc. *146*, 884–891. https://doi.org/10.1021/jacs.3c11293.